GEOLOGICA CARPATHICA, APRIL 2023, 74, 2, 139–153 https://doi.org/10.31577/GeolCarp.2023.10

Remobilization of Ni–Co–As and platinum-group elements by carbonate metasomatic alteration (listvenitization) of metaultramafic rocks from Dobšiná, Slovakia

STEFAN KIEFER[1,✉], PETER IVAN[2], ANDREAS B. KAUFMANN[1,3], MAREK VĎAČNÝ[4] and JURAJ MAJZLAN[1]

[1]Institute of Geosciences, Friedrich Schiller University, Burgweg 11, Jena, Germany; ✉Stefan.Kiefer@uni-jena.de
[2]Department of Geochemistry, Comenius University, Ilkovičova 6, Bratislava, Slovakia
[3]Institute of Mineralogy, Leibniz University, Callinstr. 3, Hannover, Germany
[4]Earth Science Institute of the Slovak Academy of Sciences, Dúbravská cesta 9, P.O.BOX 106, Bratislava, Slovakia

(Manuscript received August 3, 2022; accepted in revised form April 4, 2023; Associate Editor: Peter Koděra)

Abstract: Hydrothermal processes are mainly responsible for the release and accumulation of metals and metalloids in rocks. In this work, we investigated the mineralogy and geochemistry of altered metaultramafic rocks (listvenites) that are spatially associated with Ni–Co ores near Dobšiná aiming to identify the sources of the elements in the hydrothermal Ni–Co-mineralization. Optical microscopy, electron microprobe analysis, and laser-ablation inductively coupled plasma mass spectrometry (LA-ICP-MS) were used to correlate the mineralogy with the degree of rock alteration. The sulfides and silicates in the metaultramafic rocks host rare, tiny inclusions of cooperite (nominally PtS), sperrylite ($PtAs_2$), Pty–Pd–Ir–Te phase, and Pt–Au–Cr-alloy. The results show that the metaultramafic rocks were the source of Ni and Co and that platinum-group elements (PGE) were also leached and mobilized from the metaultramafic rocks. LA-ICP-MS scans show that the sulfarsenides in the metaultramafic rocks host submicrometer inclusions of PGE minerals but the hydrothermal Ni–Co sulfarsenides contain much less PGE's. These observations document the limited mobility of the PGE's. Changes in the sulfide mineralogy as a function of degree of alteration suggest that the fluids brought Fe and S, and probably a substantial amount of As whereas the metaultramafic rocks supplied Ni, Co, PGE, and perhaps also some As.

Keywords: hydrothermal processes, metal release, platinum-group elements, geochemistry, sulfides, sulfarsenides, Dobšiná

Introduction

Hydrothermal processes are the most effective concentrators of ore metals and metalloids. As a result of these processes, ore bodies of relatively small size, not exceeding several km^3, are formed. The conditions of the formation of such hydrothermal deposits are difficult to reconstruct due to the extraordinary complexity of the hydrothermal systems that created them. Moreover, hydrothermal system dimensions exceed the ore mineralization size several fold (Reimann et al. 2016) and are as a rule inactive – fossil at the time of investigation. Therefore, many aspects of the genesis of hydrothermal mineralization are still debated, such as the problem of the source of metals. There are, though, some hydrothermal mineralizations that are uniquely suited to provide clues in this matter. The Ni–Co deposit in the neighborhood of the small town of Dobšiná in eastern Slovakia is one of such mineralizations.

The region around the Dobšiná town is a geological knot where several superunits of the Western Carpathians meet. One of them, the Paleozoic Gemeric Superunit, belongs to the most important metallogenic provinces of the Western Carpathians. It hosts genetically variable ore deposits, with the dominant siderite–sulfide and gold–stibnite–quartz vein-type deposits (Grecula et al. 1995). Veins of both types are present in the vicinity of the Dobšiná town, but only some of siderite–sulfide veins are rich in Ni–Co arsenides and represent well-known specific type of Cu–Ni–Co mineralization (Dobšiná/Dobschau type; Schneiderhöhn 1944) intensively mined in the 19th century.

The sources of elements in these hydrothermal bodies are largely unknown. For the Ni–Co mineralization, hydrothermal-metasomatic alteration of serpentinites (so-called listvenitization) were seen as the source rocks for Ni and Co (Hovorka & Ivan 1981a; Ivan 1985). Similarly, serpentinites are seen as the source of these elements in larger hydrothermal Ni–Co deposits, such as Bou Azzer (Leblanc & Fisher 1990; Tourneur et al. 2021). The source of As, however, is less certain, although also sought in the serpentinites (Tourneur et al. 2021). The primary source of Ni, perhaps also Co, can be assigned to silicates (mostly olivine) or magmatic sulfides. Both of these mineral groups usually vanish during serpentinization and subsequent hydrothermal alteration. Mobility of Ni, Co, and other elements may be documented by the composition of newly formed spinels (Fanlo et al. 2015).

A product of metasomatic alteration of mafic and ultramafic rocks are listvenites (Rose et al. 1837), usually composed of

quartz, Ca–Fe–Mg carbonates, fuchsite (Cr-muscovite), and less abundant sulfides, arsenides, magnetite, serpentine, talc, chlorite, and relics of chromite (Fryer et al. 1979; Kerrich & Fyfe 1981; Halls & Zhao 1995; Pirajno 2013). Listvenites can be economically important since they are associated with lode Au–Ag-mineralization but also with Au–Sb, Co–Ni, or Sb–Cu mineralizations (Šoštarić et al. 2011; Zoheir & Lehmann 2011). For Au-rich systems, Zoheir & Lehmann (2011) suggested that CO_2–CH_4-rich fluids caused extensive carbonation and drop of oxygen fugacity, which then destabilized and remobilized sulfides and gold. Relics of chromite, partially altered to magnetite, have been identified as the source of PGE remobilized during the metasomatic reactions in listvenites (González-Jiménez et al. 2010; Holwell et al. 2017; Beinlich et al. 2020). Metamorphic devolatilization/dehydration reactions which involve production of carbonates and mica, deposition of gold and sulfides are most effective in mafic-ultramafic host rocks (Phillips & Powell 2010; Pirajno 2015).

In this work, we searched for geochemical and geological criteria to identify the sources of the elements in the Ni–Co mineralizations near Dobšiná. Detailed mineralogical and geochemical investigation of the opaque minerals in the listvenites that are spatially associated with the ores discerned similarities among the ores and listvenites. Identification and chemical analyses of opaque minerals by the means of optical microscopy, electron microprobe, and laser-ablation inductively coupled plasma mass spectrometry, allow to correlate mineralogy with the degree of rock alteration. Variations in mineralogy, including the mineralogy of PGE-containing minerals, point at sources of the elements and processes that remobilized them.

Geological settings

Regional and local geology

The Gemeric Superunit is a polymetamorphic terrain that presented a significant conundrum to many geologists in the past and in the present. Two different concepts of the geological structure and evolution were presented by Bajaník et al. (1983) and Grecula et al. (2011). The first concept considers the Gemeric Superunit as a product of episodic sedimentation, igneous activity and intervening hiatuses, followed by multiple metamorphic events. The second concept emphasizes the nappe structure, with the nappes being detached and stacked already during the Variscan shortening. This nappe structure was reworked and consists of several nappes, detached and stacked onto each other in times from the Variscan orogeny until the peak of the Alpine orogeny (Cretaceous) and then modified by younger faults. The entire superunit is characteristic by significant tectonic shortening and reduction. The nappes correspond to the separate lithotectonic units. The preserved record (age, lithology, magmatic and metamorphic activity) reflects the Variscan geodynamic evolution from an accretion orogen in Upper Cambrium–Ordovician, to continental rifting in Lower Devonian, ocean opening in Upper Devonian, collision and subduction in Lower Carboniferous, and post-collision stabilization of the orogen, with hints of a transition into extension regime in Upper Carboniferous to Permian (Ivan & Méres 2012; Ivan 2019; Vozárová et al. 2021, and references therein). Apart from the lower-crustal rocks in the Klátov Group (Klátov Gr.), all lithotectonic units originated in the upper-crustal conditions and did not undergo, as a whole, metamorphism that would exceed low-grade conditions. Almost all these lithotectonic units can be found in the vicinity of Dobšiná and they all host siderite–sulfide vein mineralization. Yet, the veins with rich Ni–Co mineralization are located only in the rocks of the Klátov Group or their immediate vicinity.

The Klátov Group (Hovorka et al. 1990) is made of medium- to high-grade metamorphic rocks which experienced multiple events of retrograde metamorphism. Two main types of rock complexes can be distinguished within this group, namely (1) amphibolite and (2) gneiss–migmatite. The amphibolite complex is represented by fine- to medium-grained, monotonous amphibolites, locally also banded rocks with bands of leptynite. There may be rare relics of two-pyroxene granulites and granulite-facies metacarbonates. The gneiss–migmatite complex is dominated by amphibolite gneisses, augen gneisses to migmatites with enclaves of migmatized gabbros, pyroxenites, two-pyroxene granulites, metaultramafic rocks, and retrogressively modified eclogites (Faryad et al. 2020). Thin veins of pegmatites are common. The age of migmatitization is Upper Devonian (383±3 Ma), the age of the igneous protolith is Lower Ordovician (482±9 Ma; Putiš et al. 2009). The Klátov Group was originally made of basic intrusive rocks, basic and ultrabasic rocks of subducted oceanic crust, metamorphosed and migmatized during the Devonian rifting (Ivan 2016). During exhumation and subsequent evolution, the group was affected by retrograde metamorphism in amphibolite-, blue-schist-, prehnite–pumpellyite-, and green-schist facies as well as tectonic reworking.

Our field observations show that the rocks of the Klátov Group around Dobšiná form a tabular body with lateral extent of ~3×4 km, thickness not more than 200 m, slightly dipping to south, fragmented by N–S faults into several pieces and found at its W margin only as isolated fragments (Figs. 1, 2). The footwall is made of metabasic rocks of the Rakovec Group of Devonian age, the hanging wall is made of conglomerates, sandstones, black shales, and limestones of the Upper Carboniferous Rudňany Formation. Pebbles of rocks that correspond to the content of the Klátov Group can be found in these conglomerates.

The southvergent thrusting of the Klátov Group body was accompanied by formation of steep shear faults with intensive mylonitization (Rozložník 1965). Gneisses and migmatitized gneisses, which contain primary graphite, were modified to black ultramylonites composed of chlorite, graphite, tourmaline, rutile, quartz, and illite. The thrusting plane itself is locally occupied by lenticular bodies of serpentinites with

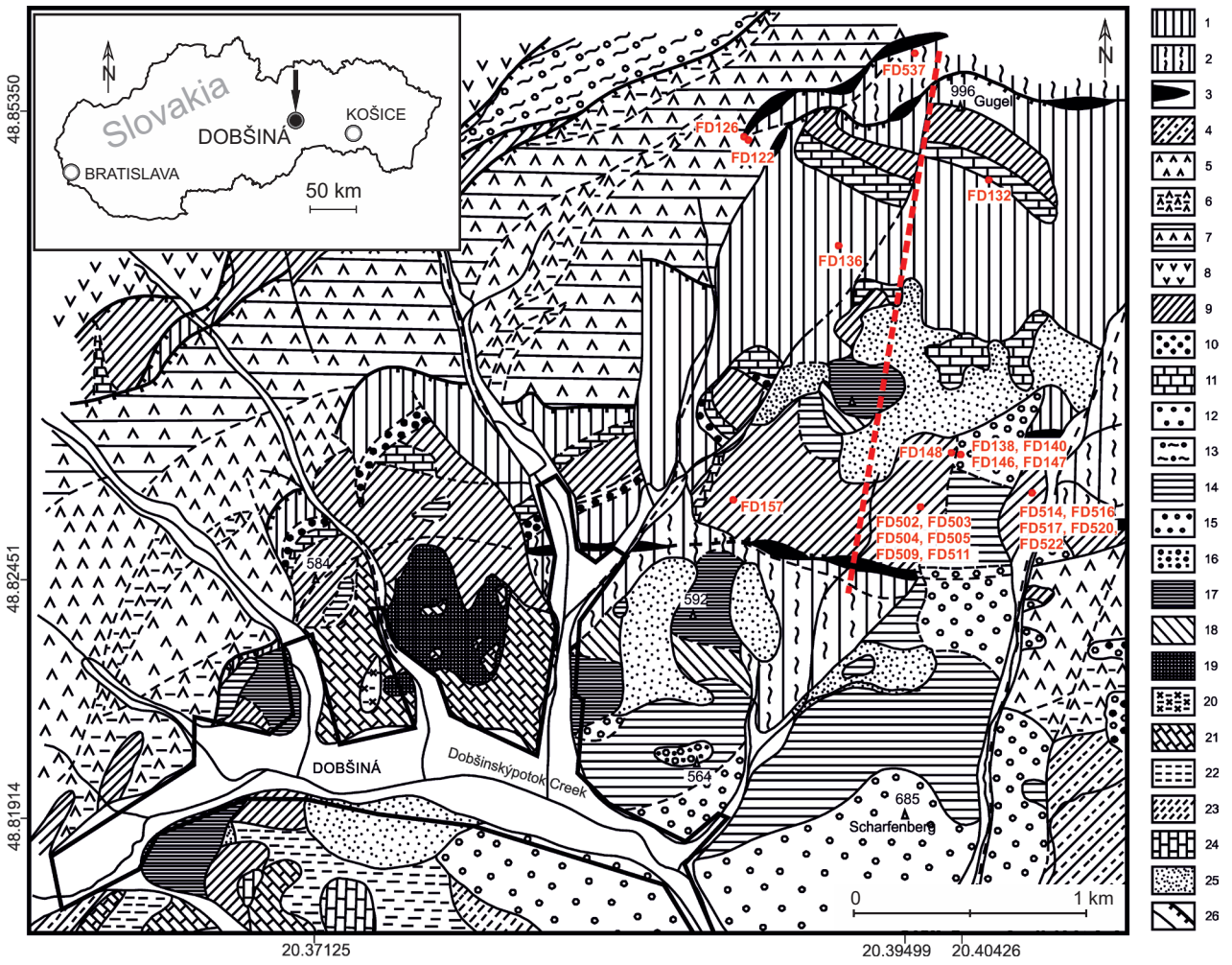

Fig. 1. Geological map of the vicinity of the Dobšiná township (modified after Hovorka & Ivan 1985, Ivan & Méres 2009, based on earlier maps of Rozložník 1956 and Bajaník et al. 1984). Explanations: 1 – amphibolites; 2 – gneisses and migmatitized gneisses; 3 – antigorite serpentinites and their hydrothermally altered equivalents (listvenites) (1–3 Klátov Gr.; Ordovician/Devonian); 4 – rhyolite metavolcaniclastics (4 Gelnica Gr.; Ordovician); 5 – metabasalts; 6 – chlorite-sericite phyllites; 7 – redeposited basaltic metatuffs intercalated by metabasalt bodies (5–7 Rakovec Gr.; Devonian); 8 – Zlatník Gr. (Upper Devonian/Lower Carboniferous); 9 – shales, black shales, sandstones; 10 – conglomerates; 11 – limestones partly metasomatically replaced by siderite (9–11 Rudňany Fm.; Upper Carboniferous); 12 – metamorphosed conglomerates; 13 – strongly mylonitized conglomerates; 14 – metamorphosed sandstones and shales (12–14 Krompachy Gr.; Permian); 15 – metamorphosed conglomerates (Gočaltovo Gr.; Permian; 1–15 Gemeric Megaunit); 16 – metamorphosed conglomerates (Jasov Fm.; Permian); 17 – metabasalts; 18 – sericite phyllites, black phyllites and metamorphosed sandstones with enclaves metamorphosed red radiolarites; 19 – lizardite-chrizotile serpentinite; 20 – acid metavolcanite; 21 – sericite phyllites with mostly marble enclaves; 22 – chlorite-sericite phyllites with marble intercalations; 23 – greenish and red sericite phyllites (16–23 Bôrka Nappe; Upper Triassic–Upper Jurassic(?); Meliatic Megaunit); 24 – Gutenstein-type dolomites; Middle Triassic; Silicic Megaunit); 25 – debris; 26 – faults, thrusts. The red dashed line shows the approximate position of the cross section in Figure 2. The red dots show the sampling location. Please note: Most of the data included in this publication were obtained from subsurface samples.

thickness of several tens of meters. Owing to their low yield strength, these rocks were pressed into some fault zones and form vein-like bodies (Hovorka & Ivan 1985).

The veins with Ni–Co ore mineralization are mostly located in the steep faults in the N and S flanks of the Klátov Group body. They are parallel to the thrusting plane with the metaultrabasic rocks, less commonly, they are located near the thrusting plane (Grecula et al. 1995 and references therein). At the northern flank, the veins have variable thickness (0.1 to 2 m), are hosted in gneisses and migmatitized gneisses, especially in the black mylonites in these rocks. In amphibolites, the veins are thinner. The veins at the southern flanks are hosted in strongly altered rocks – gneisses, amphibolites, or metaultrabasic rocks. The veins are much thinner (0.1 to 0.5 m) and with smaller extent.

The veins are made of carbonates (Fe-dolomite, ankerite, siderite), quartz, Ni–Co–Fe sulfarsenides (gersdorffite, arsenopyrite). In the higher portions of the veins, Ni–Co minerals become less common and sulfides are represented by chalcopyrite and tetrahedrite. The veins at the southern flank of the Klátov Group body have higher Ni/Co ratios than those at the northern flank. Mineralogy of the Ni–Co veins from

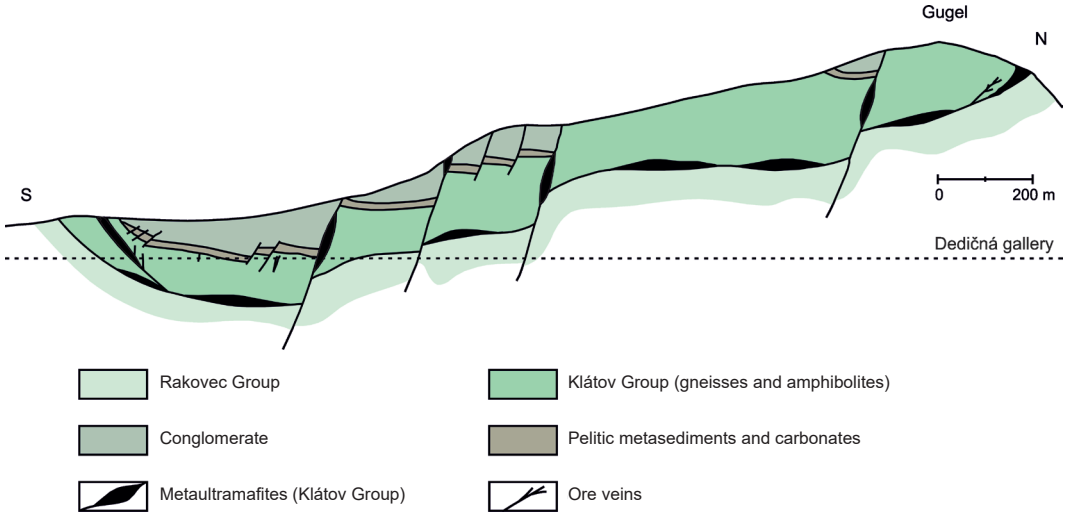

Fig. 2. Geological profile of the rock complexes that host the hydrothermal Ni–Co veins and the Klátov Group serpentinites near Dobšiná.

Dobšiná was studied in detail by Halahyjová-Andrusovová (1961), Kiefer et al. (2017), and Števko & Sejkora (2020). Geochronological (Re–Os) data document the Cretaceous age of the mineralization (Kiefer et al. 2020; Majzlan et al. 2022), in agreement with the age of the youngest metamorphic event and tectonic activity in this area (Lexa et al. 2003) but are in conflict with metallogenetic concepts of Radvanec & Grecula (2016). The mineralization is accompanied by strong hydrothermal-metasomatic overprint of the host rocks. In this process of listvenitization, the amphibolites and gneisses were transformed into chlorite–quartz–carbonate, illite–quartz–carbonate, and illite–carbonate rocks. Locally, the gneisses underwent also intensive silicification.

Uppermost parts of the Ni–Co mineralization reached the overlying Lower Carboniferous rocks. Here, the metasomatic siderites (formed by replacement of the limestone protolith) contain accumulations or veinlets of Ni–Co minerals. Listvenitized metaultrabasic rocks were found at places, likely dragged to their current position along the faults. The veins at the northern flank penetrate into the overlying Carboniferous sediments but once they do, they are devoid of Ni–Co minerals and contain instead only siderite, baryte, tetrahedrite, and cinnabar.

Serpentinites in the Gemeric and Meliatic superunits in Dobšiná

There are two distinct types of metaultramafic rocks in the vicinity of Dobšiná. They differ in their mineral composition and association to the large geological units of the Western Carpathians. The first type are antigoritic metaultramafic rocks of the Klátov Group of the Gemeric Superunit (Hovorka & Ivan 1981b). The Klátov Group metaultramafic rocks succumbed almost completely to intensive listvenitization, with the exception of small bodies and ultramafic balls enclosed in gneisses. A detailed petrographic description of these rocks and their alteration products can be found in the Results section of this publication.

Another metaultramafic body in Dobšiná, mined in the past in a quarry for asbestos (Fig. 1), will be referred to as the Meliatic serpentinites. These are Triassic chrysotile serpentinites (Hovorka et al. 1985) and they belong to the ophiolite-bearing polygenic mélange of the Meliatic Superunit. These rocks contain dispersed opaque phases (Rojkovič & Hovorka 1979) and host minor Ni–Co mineralization (Števko et al. 2013).

Samples and methods

A total of 21 samples of Klátov Group serpentinites and listvenites were collected in the vicinity of Dobšiná. Samples were found in the Tešnárky Valley, around the Gugel and Langenberg hills, and from the bore hole VD-20.

Another set of 5 samples comes from the historical collection of Dr. Halahyjová-Andrusovová. These samples were collected from the hydrothermal veins and present rich Ni–Co mineralization. They were used for a detailed mineralogical study by Kiefer et al. (2017) who also reported their localization.

Samples were prepared in the form of thin and polished sections and examined in transmitted and reflected polarized light. Sections with abundant opaque phases were selected for further analyses with electron microprobe (EMP) or laser ablation inductively-coupled plasma mass spectrometry (LA-ICP-MS).

Electron microprobe

Textural and compositional relationships were further investigated by electron microprobe analyses using a JEOL JXA-8230. The operating conditions were set to an accelerating

voltage of 20 kV, a beam current of 100 nA and a beam diameter between 1–5 μm. The wavelength-dispersive X-ray spectrometers were used to measure the elements and X-ray lines of Sb (Lα), S (Kα), As (Kα), Zn (Kα), Cr (Kα), Co (Kα), Cu (Kα), Ni (Kα), Fe (Kα), Au (Mα), Pd (Mα) as well as Te (Lα) and Ir (Mα) (for one measurement). To improve the count-rate statistics, the counting times were 600 s for Pt, Pd, and Ir, 200 s for Te and Au, and 40 s for the other elements. The standard specimens used for calibration were pure metal standards (100 %) for Pt, Pd, Ir, Au, Ni, and Co, stibnite for Sb, pyrite for Fe and S, arsenopyrite for As, chromite for Cr, sphalerite for Zn, and chalcopyrite for Cu. Peak overlap correction was used to avoid interference between the lines of Pt and Sb, Au and Pt, Fe and Pt, Co and Pd, S and Co, As and Ir, Cr and Ir, Cu and Ir as well as Cr and Au. The detection limits, calculated from the peak and background counts, the measurement time, the beam current, and the standard material concentration, are (in wt. %): 0.01 for Pt, S, Co, Fe, and Pd, 0.02 for Ni, Cr, and Cu, 0.03 for Sb and Ir, 0.04 for Zn, Au, and Te, and 0.05 for As.

Whole rock geochemistry

For trace-element geochemistry, 22 samples were ground, digested in aqua regia and analyzed by inductively coupled plasma mass spectrometry. Elements analyzed and detection limits (on weight basis) were: Cu (0.01 ppm), Zn (0.1 ppm), Ag (2 ppb), Ni (0.1 ppm), Co (0.1 ppm), Fe (0.01 %), As (0.1 ppm), Au (0.2 ppb), Bi (0.02 ppm), Cr (0.5 ppm), Ti (0.001 %), S (0.02 %), Te (0.02 ppm), Pd (10 ppb), and Pt (2 ppb). A few selected samples were additionally analyzed for all platinum-group elements by instrumental neutron-activation analysis. The elements analyzed and their detection limits were Ir 1 ppb, Os 10 ppb, Rh 5 ppb, Ru 50 ppb.

LA-ICP-MS

The determination of trace element analyses was performed using an Element XR (Thermo Scientific, Germany) fast-scanning sector field ICP-MS coupled to a femtosecond laser ablation (fs-LA) system (Solstice, Spectra-Physics, USA) at the Institute of Mineralogy, Leibniz University, Hannover, Germany. Laser operates in the deep UV at 194 nm that produces energy pulses of 70–90 mJ. Measurements were performed using a laser beam of 60 μm with a repetition rate of 18 Hz for standards and 40–60 μm spot size and repetition rate between 16–50 Hz for samples. Ablated particles were transported from the sample chamber by He carrier gas and mixed with Ar before entering the Element XR. A Jet sample cone and a skimmer X cone were used (material composed of Ni) in combination with a 1 mm copper ring (spacer). During tuning, the oxidation rate formation was limited to a ThO/Th value ≤0.5 %. The external reference standards were NIST SRM 610 (Jochum et al. 2011) and PGE-A (Gilbert et al. 2013). The Ni, Sb, Fe, and Cu concentrations of the minerals determined by EPMA were used as internal standards for quantification. Different elements were used as internal standards due to different sample matrix and sample heterogeneity. The PGE-A standard was used as quality control material. The reproducibility of the trace elements was better than 20 %. Data were reduced and drift corrected, using a Matlab-based SILLS program (Guillong et al. 2008). Argide interference on the light PGE isotopes (^{99}Ru, ^{101}Ru, ^{103}Rh, ^{105}Pd, and ^{106}Pd) and silver (^{107}Ag) was corrected by measuring Co-rich pyrite, millerite (NiS), chalcopyrite ($CuFeS_2$), native Cu, CdS, and sphalerite (ZnS) reference materials. The argide interference level was determined by measuring of the pure metals and the obtained interference level was subtracted from the sample, to obtain the argide free sample concentration.

Results

Petrography of the Klátov Group metaultramafic rocks and their listvenitization products

The least altered metaultramafic rocks are represented by antigorite serpentinites with typical arborescent texture, rarely with relics of the meshwork texture from the earlier lizardite–chrysotile serpentinization event. The primary rocks were most likely mantle peridotites. The antigorite serpentinites are composed mostly of antigorite, with a lesser amount of magnetite, Mg-chlorite, and tremolite. Already before antigoritization, the euhedral magmatic Cr-spinel was replaced by magnetite or metamorphosed to chromite. The released Mg and Al were taken up by chlorite. The spinel grains were intensively crushed. Sulfide minerals are represented by pentlandite and millerite. Scarce carbonates replace antigorite but they are related to the younger alteration events. Rare metaultramafic balls in gneisses were completely changed to talc and have a reaction rim (black wall) that consists of monomineral zones of tremolite, chlorite, sometimes also phlogopite.

Listvenitization of the antigorite serpentinite proceeded as a gradual loss of some minerals and their replacement by newly formed mineral assemblages. The final result is a sequence of metasomatic zones, separated from each other by relative sharp interfaces. An ideal sequence of such zones is displayed in Fig. 3 (Ivan 1985, 1987) and is essentially identical to the sequence determined as listvenite sites in the Ural Mountains (Sazonov 1975).

The first listvenitization stage was a response to influx of fluids with CO_2 but with little Fe and generated the following metasomatic products: antigorite–talc–carbonate rocks → talc–carbonate rocks → chlorite–quartz–carbonate rocks → fuchsite–quartz–carbonate rocks.

In the antigorite–talc–carbonate rocks, talc and carbonates formed at the expense of antigorite and the proportions of all three minerals are roughly equal. These rocks are usually massive, the original arborescent texture is largely obliterated. The talc–carbonate rocks lost all antigorite and the proportions of talc and carbonates are roughly equal. Some of these rocks

are distinctly foliated. Listvenites sensu stricto include the chlorite–quartz–carbonate and fuchsite–quartz–carbonate rocks with pronounced foliation and predominance of carbonates over quartz. Chlorite and fuchsite represent only a few per cent of the samples. The only mineral of the primary igneous rocks that persisted in this stage of listvenitization is chromite (or the relics thereof). Already the initial carbonate replacement is accompanied by dissolution of the magnetite rims on chromite. Chlorite, formed during the intermediate listvenitization, is later replaced by talc and then by carbonates. Chlorite aggregates were stretched into minute lenses or veinlets, whereas chromite was crushed and replaced by other minerals. Fuchsite is usually the final replacement product of chlorite but chromite relics persist even this alteration. Chemical composition of the carbonates is variable. Fluids that brought no Ca caused precipitation of Fe-magnesite. In other cases, the carbonates are both Fe-magnesite and dolomite or only dolomite.

In the second stage of listvenitization, the fluids brought Fe and replaced the carbonates in the earlier listvenites (Fe-magnesite and dolomite) by siderite. The result are fuchsite–quartz–siderite listvenites with such predominance of siderite that these rocks were exploited as metasomatic Fe ores. Locally, especially near to siderite veins, listvenites were intensively silicified and altered to fuchsite–quartz rocks (Ivan 1985). Despite variable, medium to strong alteration, the protolith can be always tracked and identified by the relics of chromite in these rocks.

Chemical composition of the rocks also varied during listvenitization. The earliest products (antigorite–talc–carbonate and talc–carbonate rocks) maintained the principal chemical features of the protolith (Ivan 1985), namely high MgO, Cr, Ni, and Co content, but with addition of CO_2. In some of them, the MgO concentrations are diminished at the expense of CaO. The listvenites sensu stricto (chlorite–quartz–carbonate and fuchsite–quartz–carbonate rocks) have distinctly less Ni and Co, probably as a consequence of the replacement of the Mg-silicates by carbonates. Upon the replacement of siderite, the Ni and Co concentrations decrease once again. The concentration of Cr is slowly falling as the listvenitization proceeds and is related to the degree of dissolution of chromite. These concentrations, however, remain high and attest to the limited mobility of Cr during listvenitization (Ivan 1985).

The studied metaultramafic rocks are fine-grained and massive, sometimes foliated as the result of flattening and shearing. Mineralogical and chemical changes as a function of progressive listvenitization were described in detail above and are graphically summarized in Fig. 3.

Mineralogy of opaque phases

Chromite is a characteristic accessory mineral and was found in every sample used in this work in different proportions. There is a negative correlation between abundance of chromite and the alteration degree of listvenites. The more altered samples have in general less chromite, but exceptions from this trend are common. In the serpentinites, chromite is less altered and the chromite clusters are up to 2 cm in diameter. On the other hand, chromite in the listvenites shows sponge texture caused by the intensive metasomatic reactions. Sometimes chromite is overgrown by magnetite. Some listvenite samples contain zones with quartz, dolomite, illite, and abundant rutile.

The investigated antigoritic serpentinites contain no sulfides or other ore minerals apart from chromite and magnetite. The listvenites contain abundant small (<100 μm) disseminated accumulations of opaque, sulfide–arsenide minerals (Figs. 4, 5). Overall, they are minor to trace constituents of these rocks. Their identification is challenging due to the size of the minerals and their complex intergrowths. Nevertheless, it was possible to identify pyrite, chalcopyrite, arsenopyrite, gersdorffite, skutterudite, pentlandite, siegenite, linnaeite, and millerite by reflected-light microscopy (Fig. 4).

The most common sulfides in the listvenites are millerite and siegenite, usually intergrown with each other (Figs. 4a, 5a) in anhedral grains. Gersdorffite and other sulfarsenides are usually found disseminated in the silicates of the listvenites or overgrowing sulfides (Fig. 5b). Pyrite occurs in almost all samples in different sizes and shapes (anhedral to euhedral).

Sulfides of Ni–Co–Fe show certain correlation with the degree of rock alteration. The more distal zones contain more millerite and siegenite than the proximal zones. Millerite and siegenite are found especially in the antigorite–talc–carbonate and talc–carbonate rocks. Pyrite is present in all listvenite samples, but its proportion increases toward the proximal zones. Here, pyrite is accompanied by minor amount of siegenite, but millerite is missing.

PGE minerals form tiny grains found in chlorite–quartz–carbonate, fuchsite–quartz–carbonate, and fuchsite–quartz rocks. They all belong to the listvenites with higher degree of metasomatic overprint. The minerals of PGE are spatially associated with sulfides (e.g., pyrite) but may be also enclosed in silicate matrix (e.g., fuchsite) with no opaque minerals.

Sulfarsenides of the gersdorffite–cobaltite series are restricted to the most proximal alteration zones and in the hydrothermal veins themselves. They were found in the chlorite–quartz–carbonate and fuchsite–quartz–carbonate rocks.

Chemical composition of the opaque minerals – electron microprobe

Pyrite, chalcopyrite, and tetrahedrite

Pyrite in the listvenites shows stoichiometric compositions with low amounts of As, Ni, and Co with a mean formula $Fe_{0.97}Co_{0.01}Ni_{0.02}S_{2.00}$. Higher Ni, Co, and Cu concentrations are restricted to irregular patches in larger pyrite crystals. The Ni-richest composition can be expressed by the formula $Fe_{0.87}Ni_{0.18}S_{1.94}$. Arsenic is slightly enriched in rims, but the concentrations are low (<1 wt.%).

Chalcopyrite is found either intergrown with Fe–Ni sulfides or as large anhedral masses together with tetrahedrite.

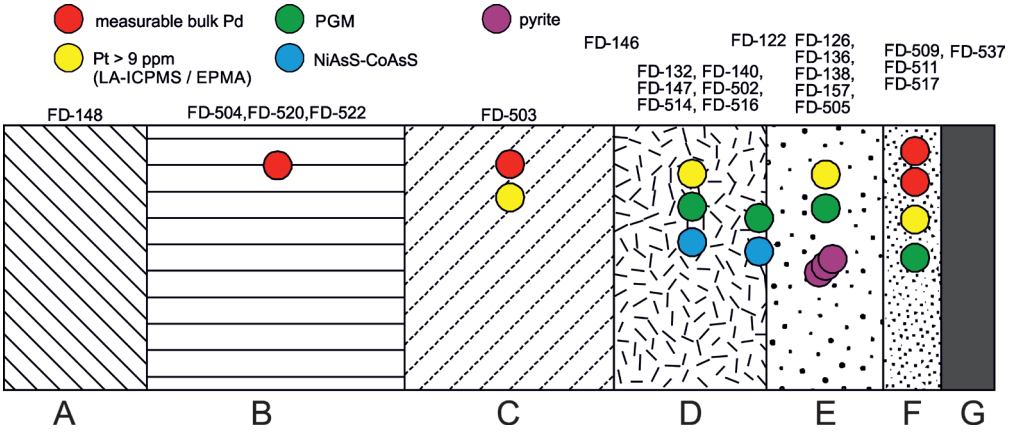

Fig. 3. Idealized profile of alterations of the antigorite serpentinites. Samples used in this study are assigned to the mineral assemblages in the alteration zones and listed on the top of the profile. Features related to the occurrence of sulfide minerals or PGE are marked by the colored circles. Each sample that contained such minerals or PGE concentrations is represented by one circle; for that reason, there may be more than one circle of a certain color in one column. Explanation: A = antigorite-serpentinites, B = antigorite–talc–carbonate rocks, C = talc–carbonate rocks, D = chlorite–quartz–carbonate rocks, E = fuchsite–quartz–carbonate rocks, F = fuchsite–quartz rocks, G = carbonates with ore minerals

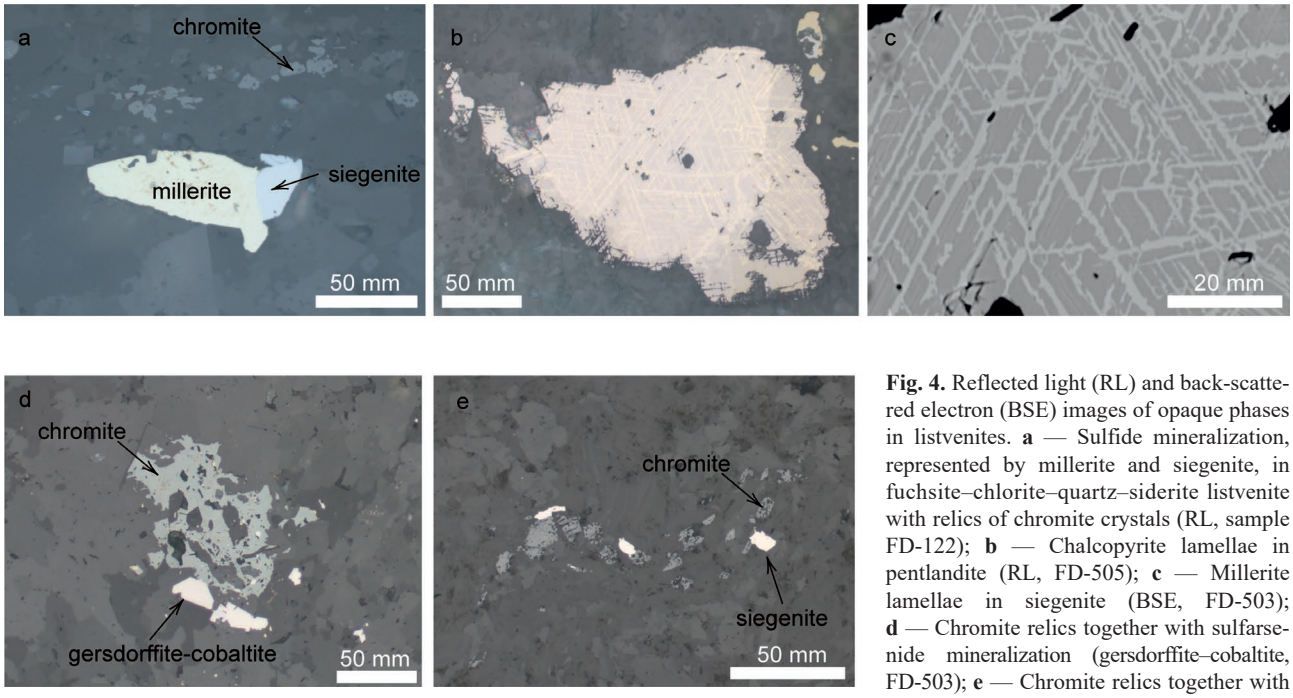

Fig. 4. Reflected light (RL) and back-scattered electron (BSE) images of opaque phases in listvenites. **a** — Sulfide mineralization, represented by millerite and siegenite, in fuchsite–chlorite–quartz–siderite listvenite with relics of chromite crystals (RL, sample FD-122); **b** — Chalcopyrite lamellae in pentlandite (RL, FD-505); **c** — Millerite lamellae in siegenite (BSE, FD-503); **d** — Chromite relics together with sulfarsenide mineralization (gersdorffite–cobaltite, FD-503); **e** — Chromite relics together with siegenite (FD-157).

The aggregates of chalcopyrite and tetrahedrite usually overgrow Ni–Co sulfarsenides. The mean composition of chalcopyrite is $Cu_{0.99}Fe_{1.00}S_{2.01}$ and the only trace elements are Sb and As (up to 0.07 and 0.09 wt.%) in assemblages with tetrahedrite and Ni (up to 0.08 wt.%) in assemblages with the Fe–Ni sulfides.

Siegenite, millerite, and pentlandite

Siegenite and millerite usually occur together (Figs. 4a, 5a). Millerite is chemically homogeneous (Table 1), with minor Fe (up to 1.05 wt.%), Co (0.16), and As (0.14). The composition of siegenite is more variable, with a tendency to be As-richer and S-poorer than the nominal formula, with the mean formula $Ni_{2.13}Fe_{0.11}Co_{0.65}Cu_{0.01}S_{3.91}$.

Pentlandite is only a minor phase with the mean stoichiometry $Ni_{4.32}Fe_{4.43}S_{8.18}$ displaying a Fe:Ni-ratio of (almost) 1:1 and a sulfur content, which is greater than the stoichiometric amount. However, there are also some compositions with Ni:Fe ratios of almost 2:1. Apart of traces of Zn, Co, and Cu, pentlandite contains up to 0.99 wt.% Pt in spot analyses.

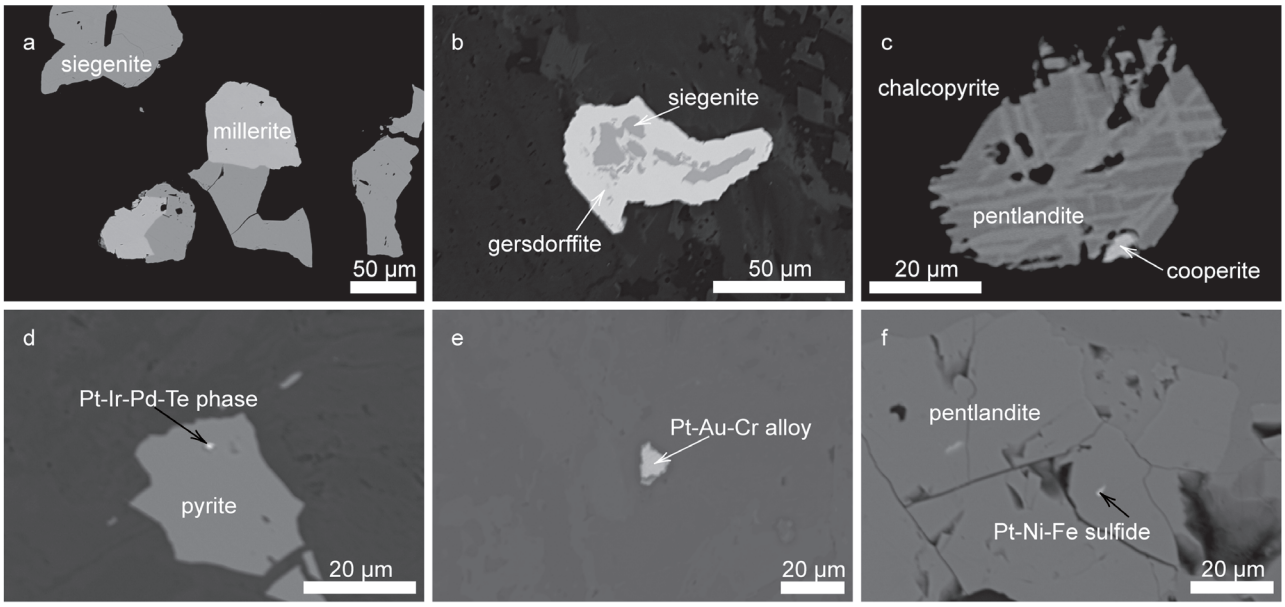

Fig. 5. Back-scattered electron (BSE) images of opaque phases in listvenites. **a** — Disseminated sulfide grains in quartz–dolomite listvenite (sample FD-138); **b** — Gersdorffite rims and replaced siegenite in fuchsite–chlorite–quartz–siderite listvenite (FD-122); **c** — Cooperite grain in pentlandite and chalcopyrite (FD-505); **d** — Inclusion of Pt–Ir–Pd–Te phase in pyrite, enclosed in siderite (FD-138); **e** — Inclusion of Pt–Au–Cr alloy in siderite and quartz (FD-122); **f** — Inclusion of Pt–Ni–Fe sulfide in pentlandite (FD-138).

An interesting feature of the sulfides are the exsolution textures found in the anhedral sulfide grains (Figs. 4b, c, 5c). More often are these textures formed by lamellae of millerite in siegenite, less common are lamellae of chalcopyrite in pentlandite.

Sulfarsenides and arsenides

Arsenopyrite is a minor phase and only occurs as disseminated crystals in siderite–ankerite–quartz veins together with gersdorffite. The mineral chemistry of arsenopyrite is relatively constant and approaches the mean stoichiometry of $Fe_{1.01}Co_{0.03}As_{0.97}S_{0.99}$.

Members of the gersdorffite–cobaltite solid solution (Table 1) usually occur as small disseminated crystals in the listvenite samples. They are found either together with arsenopyrite or as veinlets or are intergrown with pyrite, millerite, and siegenite (Fig. 5b). The compositions of gersdorffite–cobaltite vary from almost end member gersdorffite $Ni_{0.94}Co_{0.08}Fe_{0.02}As_{0.93}S_{1.02}$ to solid solution compositions like $Ni_{0.55}Co_{0.46}Fe_{0.04}As_{0.94}S_{1.01}$ to nearly pure cobaltite $Co_{0.88}Fe_{0.08}Ni_{0.07}As_{0.97}S_{0.99}$.

Platinum-group minerals (PGM)

Visible minerals with platinum-group elements (PGE) as their essential components are rare and usually very small (from slightly less than a µm to a few µm; Fig. 5c–f). Their small size precluded observation of their optical properties in reflected polarized light. It also posed a problem for the EMP analyses because the excitation volume involved certainly a portion of the neighboring phases. The PGM's are intergrown with base-metal sulfides or found in the listvenite matrix.

In general, the PGM's are rich in platinum and it is difficult to assign them to a mineral. One grain (sample FD-140) that could have been assigned to a known mineral (Fig. 5c, Table 2) had the composition $(Pt_{0.76}Ni_{0.10}Fe_{0.07}Cr_{0.03})As_{0.04}S_{1.00}$, corresponding to cooperite. Two tiny grains (around 1 µm) enclosed in fuchsite (sample FD-517) gave mixed analyses of PGE's, As, S, and the elements expected in fuchsite. If the elements believed to belong to the surroundings are ignored, the stoichiometry corresponds roughly to sperrylite (nominally $PtAs_2$) with a minor Pd and S content. The other compositions measured probably represent mixed analyses due to the minute size of the inclusions. Sample FD-138 contained a Pt–Pd–Ir–Te-rich inclusion in pyrite (Fig. 5d, Table 2). Sample FD-122 had a few grains of a Pt–Au–Cr-alloy (Fig. 5e) with a compositional range Pt 28.76–29.42 wt.%, S 0.15–0.17 wt.%, Cr 3.28–3.47 wt.%, Au 66.08–66.34 wt.%, and Fe 0.87–1.18 wt.% (Table 2).

PGE concentration in nominally PGE-free sulfides

Beside the PGM's in the listvenites, it is possible to detect PGE's in the nominally PGE-free sulfides and sulfarsenides of the listvenite samples and in the hydrothermal Ni–Co–As mineralization in the ore veins from Dobšiná (Table 3). Among the PGE's, only Pt and sometimes Pd were detectable in our samples, despite long counting times and high sample currents used. The average concentration of Pt in the opaque minerals of the listvenites is 0.06 wt.% (n=52). There are differences

Table 1: Representative analyses of sulfides and sulfarsenides from the Dobšiná listvenite in wt.%.

	millerite	siegenite	pentlandite	pyrite	arsenopyrite	gersdorffite–cobaltite solid solution		
Sb	<0.03	<0.03	<0.03	<0.03	<0.03	0.22	0.13	<0.03
S	35.54	41.62	33.97	53.29	19.08	19.51	17.85	18.90
As	<0.05	1.13	<0.05	0.07	44.87	44.64	47.85	44.32
Co	0.13	15.13	0.53	<0.01	<0.01	2.67	11.60	30.91
Cu	<0.02	0.72	<0.02	0.59	<0.02	<0.02	<0.02	0.09
Ni	63.70	35.14	32.85	0.46	<0.02	32.92	19.43	2.43
Fe	0.69	5.57	32.07	45.56	35.05	0.75	3.88	2.61
Total	100.07	99.32	99.38	100.02	99.00	100.71	100.49	99.27

Table 2: Electron microprobe analyses of the PGE-bearing phases from the listvenites in Dobšiná in wt.%.

phase	Pt–Ir–Pd–Te phase	cooperite	Pt–Au alloy
sample	FD-138	FD-505	FD-122
figure	5d	5c	5e
Sb	0.52	<0.03	<0.03
Pt	6.16	76.58	28.98
S	42.42	16.38	0.17
As	2.91	1.66	<0.05
Zn	<0.04	<0.04	<0.04
Cr	<0.02	0.83	3.41
Co	<0.01	<0.01	<0.01
Cu	<0.02	0.08	<0.02
Au	0.10	<0.04	66.18
Ni	0.49	2.88	<0.02
Fe	34.97	1.93	1.02
Te	4.36	<0.04	<0.04
Pd	5.84	<0.01	<0.01
Ir	2.56	<0.03	<0.03
Total	100.33	100.36	99.78

between the concentration span and the mineral. The highest concentrations were found in pentlandite. Two analyses show high Pt concentrations (0.57 and 0.99 wt.%) coupled to higher Cu contents. One analysis shows 7.43 wt.% Pt and 2.02 wt.% As, perhaps owing to submicrometer inclusions of sperrylite in pentlandite. In some cases, higher Pt concentrations can be measured in siegenite (up to 0.08 wt.%) and millerite (up to 0.07 wt.%).

The occasionally measurable Pt concentrations in the sulfarsenide minerals (arsenopyrite, gersdorffite–cobaltite solid solution) in the hydrothermal samples are usually low, between 0.02 and 0.05 wt.%. The average Pt concentration in the sulfarsenides from the hydrothermal veins (gersdorffite and krutovite) is 0.05 wt.% (n=37) (Table 4). Three analyses show higher Pt concentration of 0.11 wt.%, 0.14 wt.%, and 0.24 wt.%. Measurable Pt in the veins is found only in Ni-rich sulfarsenides and arsenides. The Pt concentrations of arsenopyrite and Fe–Co-rich members of the gersdorffite–cobaltite solid solution were always below the detection limit.

Bulk concentrations of PGE in the studied rocks

The studied listvenites contain a few of the PGE's in measurable concentrations, especially Pt and Pd (Fig. 6, Table 5). The Pt concentration averages to 6 ppb, that of Pd to 16 ppb. The sample FD-511 (fuchsite–quartz listvenite) is particularly rich in Pd, even though inspection in microscope did not lead to identification of any Pd phases (only tiny sperrylite inclusions were found). Samples FD-511 and FD-138 also contained measurable Ir (5 and 3 ppb, respectively). Osmium, Rh, and Ru were always below detection limits, although we have to notice that the detection limit for Ru (50 ppb) was much higher than for the other platinum-group elements.

There is no clear pattern of enrichment or depletion of PGE throughout the metasomatic assemblages in the listvenites. Some of the samples show elevated PGE content (defined here as >9 ppb Pt or >9 ppb Pd; Fig. 3) but it is not clear to what extent are such variations caused by nugget effects. Even the least altered antigorite serpentinites contain 5 ppb Pt, only slightly below the average of all analytical data (6 ppb).

PGE+Au concentrations in selected minerals – LA-ICP-MS

Pyrite, gersdorffite–krutovite aggregates, and chromite were analyzed for their PGE content using LA-ICP-MS. The results are summarized in Fig. 7 that shows the average concentrations of the PGE's in each profile. An example of a LA-ICP-MS profile is shown in Fig. 7f. The large signal variations in the LA-ICP-MS profiles suggest that the detected concentrations are related mostly to sub-µm inclusions.

For the listvenites, the sample FD-138 from a fuchsite–quartz–carbonate rock and FD-140 from a chlorite–quartz–carbonate rock were selected for the measurements (Fig. 7c, d). The PGE concentrations are higher in pyrite than in siegenite. Pyrite crystals (FD-138) contain on average 2100 ppb Pt, 2700 ppb Pd, 1100 ppb Ir, and 1000 ppb Ru. Striking is the very low Au concentration (average 30 ppb). In siegenite, there are only a few measurable spots with Pd, Pt, Au, and Os. The maximum concentrations in pyrite and siegenite are much higher than the averages given above, but the ablation profiles show that the maxima are limited to small spots in the minerals.

Gersdorffite in the listvenites (Fig. 7d) has even more PGE's, with averages of 16,000 ppb Ru, 11,900 ppb Pd, 2600 ppb Rh, but little Pt (140 ppb). Gold is also higher than in pyrite or siegenite, on average 3800 ppb.

The measured chromite grains in the sample FD-522 (antigorite–talc–carbonate listvenite; Fig. 7e) only show elevated Pd concentrations, with an average of 3300 ppb. Low concen-

Table 3: Representative EMP analyses of nominally PGE-free sulfides and sulfarsenides from the Dobšiná listvenite in wt. %.

element	pentlandite (FD-140)	millerite (FD-122)	siegenite (FD-122)	arsenopyrite (FD-132)	gersdorffite (FD-132)
Sb	<0.03	<0.03	<0.03	0.05	0.04
Pt	0.99	0.06	0.05	0.03	0.04
S	33.54	34.61	43.24	19.54	19.57
As	<0.05	<0.05	<0.05	44.14	44.64
Zn	<0.04	<0.04	<0.04	<0.04	<0.04
Cr	<0.02	<0.02	<0.02	<0.02	<0.02
Co	0.47	0.29	17.87	0.04	0.33
Cu	1.56	<0.02	0.77	<0.02	<0.02
Au	<0.04	<0.04	<0.04	<0.04	<0.04
Ni	34.28	63.80	35.49	<0.02	34.02
Fe	29.83	0.90	2.54	35.30	<0.01
Te	<0.04	<0.04	<0.04	<0.04	<0.04
Pd	<0.01	<0.01	<0.01	<0.01	<0.01
Ir	<0.03	<0.03	<0.03	<0.03	<0.03
Total	100.66	99.67	99.98	99.14	99.57

Table 4: Representative analyses of sulfarsenides with measurable Pt concentration from the hydrothermal mineralization from Dobšiná in wt. %.

element	gersdorffite (141b)	Pt-rich inclusion in gersdorffite (436)	krutovite (119a)
Sb	0.09	0.03	0.02
Pt	0.03	0.24	0.04
S	15.26	15.78	5.99
As	48.20	47.22	62.76
Zn	<0.04	<0.04	<0.04
Cr	<0.02	<0.02	<0.02
Co	0.26	0.34	5.42
Cu	<0.02	<0.02	<0.02
Au	<0.04	<0.04	<0.04
Ni	34.92	35.28	25.82
Fe	0.34	0.20	<0.01
Total	99.10	99.08	100.06

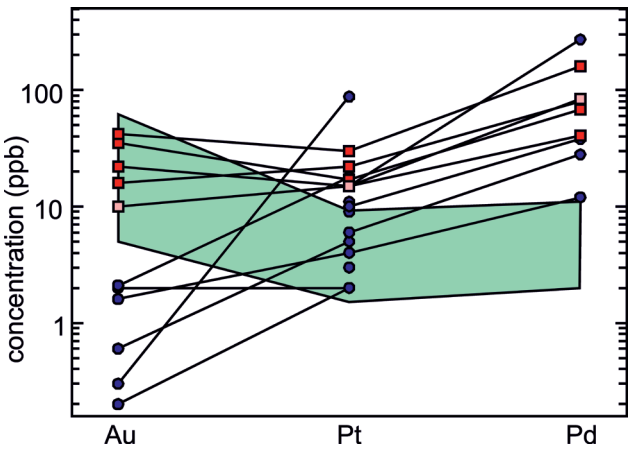

Fig. 6. Concentrations of Au, Pt, and Pd in bulk serpentinites and their listvenites from the Klátov Group serpentinites (this work, blue circles), other serpentinites in the Western Carpathians (Hovorka et al. 1983, red squares), including the Meliatic serpentinites from Dobšiná (pink squares). The pale green field shows the analytical data from serpentinites from Pohronská Polhora (F. Bakos, personal communication).

trations of Ir and Ru, just above the detection limits, were found in a few spots. Although the LA-ICP-MS profiles show clear variations in concentration, the variations are not quite so abrupt but much more homogeneous compared to the sulfides and sulfarsenides.

Gersdorffite in the hydrothermal veins has much less PGE's than the disseminated opaque phases in the listvenites (Fig. 7a, b). The average concentrations in the sample 119c are 700 ppb Ru, 100 ppb Pd, and less of the other elements. In the sample 12a, the concentrations are about one order of magnitude lower, but still dominated by Ru, with less Pd and other elements. In small spots along the measured profiles, much higher concentrations were encountered (Fig. 7f).

Discussion

Ultramafic rocks affected by hydrothermal systems and altered to listvenites serve as a source of metallic elements for ore deposits. Examples are the long-known listvenites of the Southern Ural Mts where the Au deposits with Ni–Co sulfarsenides are associated with listvenites (Belogub et al. 2017). Listvenites were postulated as the source of gold also in the Au deposits in ultramafic rocks with variable degree of listvenitization (Pipino 1980; Buisson & Leblanc 1987; Buckman & Ashley 2010; Zoheir & Lehmann 2011; Helmy & Zoheir 2015). Listvenites were also the source of Ni and Co at the Nelson deposit in New Zealand (Grapes & Challis 1999), but these authors identified a granite intrusion as the source of As.

Mineralogy of opaque phases in the Klátov Group and Meliatic metaultramafic rocks

There is a significant difference in the mineralogy of opaque phases between the Meliatic and Klátov Group serpentinites and listvenites. The Meliatic serpentinites in Dobšiná contain awaruite and heazlewoodite, with rare millerite and

pentlandite (Kantor 1955). This author reported that awaruite forms lamellae-similar aggregates and speculated that awaruite formed as a pseudomorph after an older, cubic mineral. Heazlewoodite occasionally develops a thin rim of submicrometer large grains that could be millerite but was not identified with certainty.

Awaruite and heazlewoodite are long known as witnesses of very low O_2 fugacity during serpentinization (Ramdohr 1967; Kanehira et al. 1975). They do not occur in unaltered peridotites but are common, even though minor, constituent of serpentinites. Less common are native copper (Kanehira et al. 1975) or native nickel (Dekov 2006). Extremely reducing conditions, characteristic for serpentinization, go hand in hand with very low silica activity, generating the typical mineral content of the serpentinites (Frost & Beard 2007).

Table 5: Whole rock Pd and Pt concentrations of the listvenite samples from Dobšiná. All data in ppb.

sample	Pd	Pt	Au	sample	Pd	Pt	Au
FD-122	<10	2	2.0	FD-503	<10	6	<0.2
FD-126	<10	4	1.6	FD-504	<10	4	<0.2
FD-132	<10	5	0.6	FD-505	<10	6	<0.2
FD-136	<10	2	0.2	FD-509	28	6	<0.2
FD-138	<10	11	<0.2	FD-511	273	15	<0.2
FD-140	<10	9	<0.2	FD-512	<10	3	<0.2
FD-146	38	10	<0.2	FD-514	<10	2	<0.2
FD-147	<10	5	<0.2	FD-516	<10	6	<0.2
FD-148	<10	5	<0.2	FD-520	<10	6	<0.2
FD-157	<10	3	<0.2	FD-522	12	4	<0.2
FD-502	<10	<2	<0.2	FD-537	<10	18	2.1

Preservation of awaruite and heazlewoodite in the Meliatic serpentinites excludes hydrothermal overprint and mobilization of Ni, Co, and other metals. They remained locked in the insoluble alloys. Similar, highly reducing assemblages of alloys and PGE minerals were reported from a body of Meliatic metapyroxenites in Jasov (Radvanec & Uher 2016), but only in the form of awaruite grains armored as inclusions in their silicate host.

The listvenites of the Klátov Group serpentinites, on the other hand, contain abundant sulfides and sulfarsenides in small amounts. In their early work, Hovorka & Ivan (1981a) observed millerite and pentlandite. In our work, we expanded these observations and attempted to correlate the opaque minerals with the alteration degree of the rocks.

There is a link between the mineralogy and alteration of the rocks. The arsenides and sulfarsenides are restricted to the immediate vicinity of the veins. Sulfides with higher metal/sulfur ratio, such as pyrite, are common, but their abundance drops as the alteration weakens, i.e., in the direction away from the veins. The concentrations of PGE's are higher in the listvenites than in the hydrothermal veins. These observations could be explained by leaching of Ni, Co, and PGE's from the Klátov Group serpentinites.

Sources of arsenic and sulfur for the hydrothermal Ni–Co mineralization

The possibilities of the source of arsenic are (i) sedimentary and metamorphic country rocks in the rock complexes near the ore veins, (ii) crystallization products of sulfide and

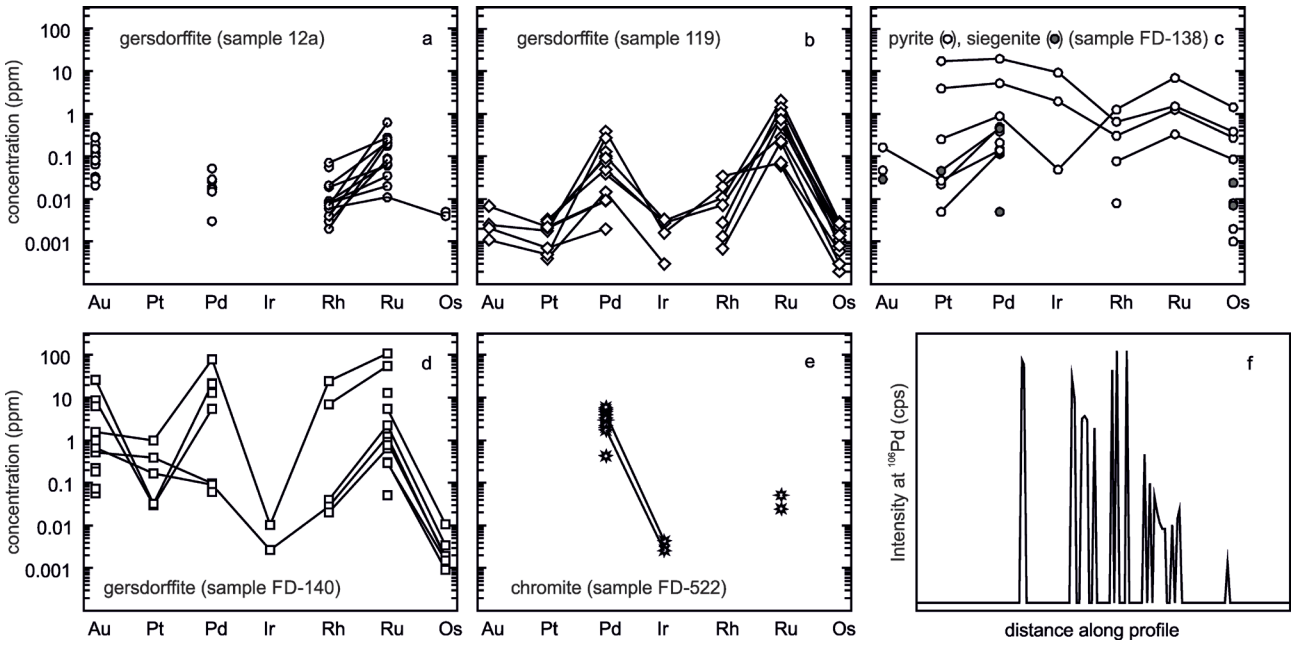

Fig. 7. a–e — LA-ICP-MS data on concentrations of PGE+Au in various minerals in the listvenite samples from Dobšiná.Vertical scales for the diagrams a–e are identical; **f** — LA-ICP-MS measurement profile on the mass 106 (palladium) in the sample 119, showing that the high concentrations are restricted to a few peaks in the data, corresponding to submicrometric inclusions of Pd-containing minerals in the sample.

arsenide melts in the ultramafic protoliths, or (iii) mantle metasomatism of the rocks.

Sedimentary rocks in the area of Dobšiná include black shales of Carboniferous age with tens of ppm of arsenic. Furthermore, there is widespread, low-grade sulfidic impregnation of the gneisses in the rock complex that hosts the veins, probably related to the retrograde, Alpine metamorphism of the gneisses in the prehnite–pumpellyite facies. These rock types could have supplied arsenic as well as sulfur into hydrothermal fluids.

Ultramafic rocks are rarely the hosts of arsenides (Ishimaru & Arai 2008) or arsenic in the oxidized, pentavalent form (Hattori et al. 2002). The highest arsenic concentrations in such rocks are restricted to specific type of orthomagmatic deposits, one of the best examples being Norilsk in Russia (Spiridonov et al. 2015). Here, one of the principal ore minerals is sperrylite ($PtAs_2$). It is assumed that the ultrabasic rocks were enriched in As and S by contamination with crustal material. In addition to the silicate melt, they also contained immiscible droplets of sulfide or perhaps arsenide melts (Piña et al. 2015, 2021). The arsenide melt has higher distribution coefficients for the PGE's than the sulfide melt and concentrates strongly the PGE's. Experimental studies on model systems confirm the observation that the Pt–Pd arsenides and antimonides crystallize at "the last dregs of crystallization" (Liu & Brenan 2015).

Arsenic, along with antimony, are relatively rapidly removed by the action of fluids from the mantle wedges during subduction; the removal from the subducting plates is somewhat slower (Hattori et al. 2002). Such fluids could have been generated during Jurassic–Cretaceous subduction and closure of the Meliata Ocean. They could have contributed to the arsenic budget of the Ni–Co veins in Dobšiná.

In a recent work, Gonzáles-Jiménez et al. (2021) investigated in detail serpentinites of the La Cabaña area in Chile. They linked precipitation of early Ni sulfides and arsenides with influx of S–As–Sb-bearing fluids during antigoritization in the subduction channel. According to this work, the trace element signature can distinguish opaque phases related to serpentinization and the orthomagmatic opaque phases. Those related to serpentinization are lower in precious metals and higher in As, Sb, Te, Bi, and Pb.

There are multiple possible sources of arsenic and other elements for the Ni–Co ores in Dobšiná. Sedimentary and metamorphic host rocks could have supplied substantial fraction of arsenic and sulfur into the hydrothermal fluids. We cannot exclude but also cannot confirm that the serpentinites themselves supplied at least some arsenic. Textural evidence shows that the sulfides are earlier than the Ni–Co sulfarsenides (Fig. 5b) and some of the sulfides may have formed during the period of antigoritization.

Bulk PGE+Au concentrations in the rocks

There are differences in the bulk concentrations of PGE+Au, when comparing the studied listvenites with other serpentinite bodies from the Western Carpathians (Fig. 6). Even though are these serpentinites of various ages and tectonic positions and the number of the available analyses is low, some trends can be discerned.

The geochemical link between the Klátov Group serpentinites and the Ni–Co mineralization is strengthened by the elevated PGE and low Au concentrations in the opaque minerals. Gold was intensively leached during listvenitization. The bulk analyses show 30–40 ppb gold in the early stages of listvenitization, dropping down to 10 ppb in the final stages (Ivan 1987). The measured Au concentrations (LA-ICP-MS) in pyrite and siegenite (from the listvenites) and gersdorffite (from ore veins) are orders of magnitude lower than those of Pd or Ru (Fig. 7). Extractions of PGE's and Au from serpentinites were also documented at the Co–Ni Bou-Azzer deposit (Morocco) (Leblanc & Fischer 1990; Tourneur et al. 2021). Many features of this large deposits are also shared by the Ni–Co mineralization in Dobšiná. Certain analogy can be also found in the mobilization and occurrence of Pd which forms a separate Bleïda deposit (within the Bou-Azzer camp; El Ghorfi et al. 2006).

These observations suggest that gold was intensively leached from the listvenites, whereas Pt, Pd, and other PGE's were not. Such behavior can be explained by much higher affinity of the PGE's for arsenides and sulfides than in the case of gold. Platinum, for example, forms a number of sulfide and arsenide minerals, such as cooperite found in this work or sperrylite assumed in this work. Gold does not have such a tendency and is carried further by the fluids, but the PGE's are captured by the sulfides and sulfarsenides in the listvenites.

Conclusions

Our results show that the metaultramafic rocks were the source of Ni and Co. The mineralogy of these elements is changing as a function of alteration degree. In the distal zones, sulfides of Ni and Co are found, whereas the proximal zones contain Ni–Co sulfarsenides.

Platinum-group elements were also leached and mobilized from the metaultramafic rocks but probably only over short distances. Their overall concentration was not affected; in the proximal zones, PGE's may have been deposited by the fluids in the form of separate minerals, albeit only as tiny grains. The LA-ICP-MS scans suggest that the sulfarsenides hosted in the metaultramafic rocks host abundant submicrometer inclusions of PGE minerals.

The hydrothermal Ni–Co ores, on the other hand, contain much less PGE's than minerals with similar chemistry and crystal structure found in the listvenites.

The sulfide mineralogy in the proximal alteration zones (pyrite, gersdorffite) suggests that the fluids brought Fe, S, and likely also substantial portion of As. We found no clear evidence that the metaultramafic rocks themselves could have been a substantial source of arsenic. An alternative

explanation, that the fluids leached As from the metaultramafic rocks almost completely and afterwards caused deposition of disseminated gersdorffite in the listvenites, is feasible but not proven. Other possible, local sources of arsenic could have been the Carboniferous black shales or gneisses with low-grade, disseminated sulfidic impregnations.

Mineralogy of the opaque phases in the Klátov Group metaultramafic rocks and the Meliatic serpentinites is completely different. Meliatic serpentinites, even though they host small hydrothermal veinlets with Ni–Co mineralization, were not altered and did not contribute material for the Ni–Co veins in Dobšiná.

Acknowledgements: This work was financially supported by a Deutsche Forschungsgemeinschaft grant KI 2131/2-1. We would like to thank Peter Koděra for editorial handling and Martin Števko and an anonymous reviewer for their helpful comments, which helped to improve the manuscript.

References

Bajaník Š., Hanzel V., Ivanička J., Mello J., Pristaš J., Reichwalder P., Snopko L., Vozár J. & Vozárová A. 1983: Explanations to the geological map of Slovenské rudohorie Mts – eastern part in the scale of 1:50,000. *State Geological Institute of Dionýz Štúr*, 1–223 (in Slovak).

Bajaník Š., Hanzel V., Ivanička J., Mello J., Pristaš J., Reichwalder P., Snopko L., Vozár J. & Vozárová A. 1984: The geologic map of the Slovenské Rudohorie Mts, eastern part, 1:50,000. *State Geological Institute of Dionýz Štúr*, Bratislava.

Beinlich A., von Heydebrand A., Klemd R., Martin L. & Hicks J. 2020: Desulphurisation, chromite alteration, and bulk rock PGE redistribution in massive chromitite due to hydrothermal overprint of the Panton Intrusion, east Kimberley, Western Australia. *Ore Geology Reviews* 118. https://doi.org/10.1016/j.oregeorev.2019.103288

Belogub E.V., Melekestseva I.Yu., Novoselov K.A., Zabotina M.V., Tret'yakov G.A., Zaykov V.V. & Yuminov A.M. 2017: Listvenite-related gold deposits of the South Urals (Russia): A review. *Ore Geology Reviews* 85, 247–270. https://doi.org/10.1016/j.oregeorev.2016.11.008

Buckman S. & Ashley P.M. 2010: Silica-carbonate (listwanites) related gold mineralisation associated with epithermal alteration of serpentinite bodies. In: New England Orogen 2010. *University of New England*, 94–105. https://ro.uow.edu.au/scipapers/715

Buisson G. & Leblanc M. 1987: Gold in mantle peridotites from Upper Proterozoic ophiolites in Arabia, Mali, and Morocco. *Economic Geology* 82, 2091–2097. https://doi.org/10.2113/gsecongeo.82.8.2091

Dekov V. 2006: Native nickel in the TAG hydrothermal field sediments (Mid-Atlantic Ridge, 26°N): Space trotter, guest from mantle, or a widespread mineral, connected with serpentinization? *Journal of Geophysical Research* 111 (B5). https://doi.org/10.1029/2005JB003955

El Ghorfi M., Oberthür T., Lüders V., El Boukhari A., Melcher F., Maacha L., Ziadi R. & Baoutoul H. 2006: Gold–palladium mineralisation at Bleïda Far West, Bou Azzer–El Graara Inlier, Anti-Atlas, Morocco. *Mineralium Deposita* 41, 549–564. https://doi.org/10.1007/s00126-006-0077-3

Fanlo I., Gervilla F., Colás V. & Subiás I. 2015: Zn-, Mn- and Co-rich chromian spinels from the Bou-Azzer mining district (Morocco): Constraints on their relationship with the mineralizing process. *Ore Geology Reviews* 71, 82–98. https://doi.org/10.1016/j.oregeorev.2015.05.006

Faryad S.W., Ivan P. & Jedlicka R. 2020: Pre-Alpine high-pressure metamorphism in the Gemer unit: mineral textures and their geodynamic implications for Variscan Orogeny in the Western Carpathians. *International Journal of Earth Sciences* 109, 1547–1564. https://doi.org/10.1007/s00531-020-01856-2

Frost B.R. & Beard J.S. 2007: On silica activity and serpentinization. *Journal of Petrology* 48, 1351–1368. https://doi.org/10.1093/petrology/egm021

Fryer B.J., Kerrich R., Hutchinson R.W., Peirce M.G. & Rogers D.S. 1979: Archaean precious-metal hydrothermal systems, Dome Mine, Abitibi Greenstone Belt. I. Patterns of alteration and metal distribution. *Canadian Journal of Earth Sciences* 16, 421–439. https://doi.org/10.1139/e79-040

Gilbert S., Danyushevsky L., Robinson P., Wohlgemuth-Ueberwasser C., Pearson N., Savard D., Norman M. & Hanley J. 2013: A comparative study of five reference materials and the Lombard meteorite for the determination of the platinum-group elements and gold by LA-ICP-MS. *Geostandards and Geoanalytical Research* 37, 51–64. https://doi.org/10.1111/j.1751-908X.2012.00170.x

González-Jiménez J.M., Gervilla F., Kerestedjian T. & Proenza J.A. 2010: Alteration of Platinum-Group and Base-Metal Mineral Assemblages in Ophiolite Chromitites from the Dobromirtsi Massif, Rhodope Mountains (Bulgaria). *Resource Geology* 60, 315–334. https://doi.org/10.1111/j.1751-3928.2010.00138.x

González-Jiménez J.M., Piña R., Saunders J.E., Plissart G., Marchesi C., Padrón-Navarta J.A., Ramón-Fernandez M., Garrido L.N.F. & Gervilla F. 2021: Trace element fingerprints of Ni–Fe–S–As minerals in subduction channel serpentinites. *Lithos* 400, 106432. https://doi.org/10.1016/j.lithos.2021.106432

Grapes R.H. & Challis G.A. 1999: Gersdorffite with pentlandite, violarite, pyrrhotite, and pyrite, northwest Nelson, New Zealand, *New Zealand Journal of Geology and Geophysics* 42, 189–204. https://doi.org/10.1080/00288306.1999.9514839

Grecula P., Abonyi A., Abonyiová M., Antaš J., Bartalský B., Bartalský J., Dianiška I., Drnzík E., Ďuďa R., Gargulák M., Gazdačko Ľ., Hudáček J., Kobulský J., Lörincz L., Macko J., Návesňák D., Németh Z., Novotný L., Radvanec M., Rojkovič I., Rozložník L., Rozložník O., Varček C. & Zlocha J. 1995: Mineral deposits of the Slovak Ore Mountains. *Geocomplex*, Bratislava, 1–834.

Grecula P., Kobulský J., Gazdačko Ľ., Németh Z., Hraško Ľ., Novotný L., Maglay J., Pramuka S., Radvanec M., Kucharič Ľ., Bajtoš P. & Záhorová Ľ. 2011: Explanations to the geological map of Spišsko-gemerské rudohorie Mts 1:50 000. *GÚDŠ*, 1–308 (in Slovak).

Guillong M., Meier D.L., Allan M.M., Heinrich C.A. & Yardley B.W. 2008: Appendix A6: SILLS: A MATLAB-based program for the reduction of laser ablation ICP-MS data of homogeneous materials and inclusions. *Mineralogical Association of Canada Short Course* 40, 328–333.

Halahyjová-Andrusovová G. 1961: Mineralogical and paragenetic study of ore deposits around Dobšiná. *Unpublished report*, *Comenius University*, Bratislava, 1–334 (in Slovak).

Halls C. & Zhao R. 1995: Listvenite and related rocks: perspectives on terminology and mineralogy with reference to an occurrence at Cregganbaun, Co. Mayo, Republic of Ireland. *Mineralium Deposita* 30, 303–313. https://doi.org/10.1007/BF00196366

Hattori K.H., Arai S. & Clarke D.B. 2002: Selenium, tellurium, arsenic and antimony contents of primary mantle sulfides. *Canadian Mineralogist* 40, 637–650. https://doi.org/10.2113/gscanmin.40.2.637

Helmy H. & Zoheir B. 2015: Metal and fluid sources in a potential world-class gold deposit: El-Sid mine, Egypt. *International Journal of Earth Sciences* 104, 645–661. https://doi.org/10.1007/s00531-014-1094-6

Holwell D.A., Adeyemi Z., Ward L.A., Smith D.J., Graham S.D., McDonald I. & Smith J.W. 2017: Low temperature alteration of magmatic Ni–Cu–PGE sulfides as a source for hydrothermal Ni and PGE ores: A quantitative approach using automated mineralogy. *Ore Geology Reviews* 91, 718–740. https://doi.org/10.1016/j.oregeorev.2017.08.025

Hovorka D. & Ivan P. 1981a: A hydrothermal leaching of an ultrabasic body – a determinant phenomenon of the Co-Ni arsenides vein deposit genesis Dobšiná, the West Carpathians. In: UNESCO International Symp. Metallog. Mafic and Ultramafic Complexes: East Mediterr., West Asia Area and com. similar Metallog. Environm. World. *UNESCO*, Athens, 172–184

Hovorka D. & Ivan P. 1981b: Serpentinite in the Paleozoic near Dobšiná. In: Bajaník Š. & Hovorka D. (Eds.): Paleovolcanism of the Western Carpathians. Bratislava, 67–78 (in Slovak with English summary).

Hovorka D. & Ivan P. 1985: Meta-ultrabasites in the Paleozoic of the inner Western Carpathians: Implications for the reconstruction of the tectonic evolution in this region. *Ofioliti* 10, 317–328.

Hovorka D., Chitrov V.G. & Rojkovič I. 1983: The content of Pt, Pd, Rh, Ru, and Au in some types of ultramafic rocks of Western Carpathians. *Mineralia Slovaca* 12, 267–273 (in Slovak).

Hovorka D., Ivan P., Jaroš J., Kratochvíl M., Reichwalder P., Rojkovič I., Spišiak J. & Turanová L. 1985: Ultramafic rocks of the Western Carpathians, Czechoslovakia. *State Geological Institute of Dionýz Štúr*, Bratislava,1–258.

Hovorka D., Ivan P. & Spišiak J. 1990: Lithology, petrology, metamorphism and tectonic position of the Klátov Group (Paleozoic of Gemeric Unit, inner Western Carpathians). *Acta Geologica et Geographica Universitatis Comenianae, Geologica* 45, 45–68

Ishimaru S. & Arai S. 2008: Arsenide in a metasomatized peridotite xenolith as a constraint on arsenic behavior in the mantle wedge. *American Mineralogist* 93, 1061–1065. https://doi.org/10.2138/am.2008.2746

Ivan P. 1985: Hydrothermally-metasomatic alterations of ultrabasic rocks. In: Hovorka D., Ivan P., Jaroš J., Kratochvíl M., Reichwalder P., Rojkovič I., Spišiak J. & Turanová L.: Ultramafic rocks of Western Carpathians, Czechoslovakia. *State Geological Institute of Dionýz Štúr*, Bratislava, 171–180

Ivan P. 1987: Gold in listvenites from sulphide-siderite Rudňany and Dobšiná deposits (Gemericum) – preliminary data. In: Gold in Western Carpathians. *State Geological Institute of Dionýz Štúr*, Bratislava, 101–110 (in Slovak).

Ivan P. 2016: The Klátov Group – unique rock complex of lower crustal origin: results of geochemical-petrologic investigation. In: Slaninka I., Jurkovič Ľ. & Ďurža O. (Eds.): Geochémia 2016. *State Geological Institute of Dionýz Štúr*, Bratislava, 60–63 (in Slovak).

Ivan P. 2019: A new concept of the geological structure of the Gemeric Superunit: study of the magmatic record using geochemical data. In: Jurkovič Ľ., Slaninka I. & Kordík J. (Eds.): Geochémia 2019. *State Geological Institute of Dionýz Štúr*, Bratislava, 82–85 (in Slovak).

Ivan P. & Méres Š. 2009: Olistholite of blueschist-facies metamorphic rocks in the Dobšiná serpentinite quarry – the proof of the link of the ultrabasic body to the Hačava formation of the Bôrky nappe. *Mineralia Slovaca* 41, 407–418 (in Slovak).

Ivan P. & Méres Š. 2012: The Zlatník Group – Variscan ophiolites on the northern border of the Gemeric Superunit (Western Carpathians). *Mineralia Slovaca* 44, 39–56.

Jochum K.P., Weis U., Stoll B., Kuzmin D., Yang Q., Raczek I., Jacob D.E., Stracke A., Birbaum K., Frick D.A., Günther D. & Enzweiler J. 2011: Determination of reference values for NIST SRM 610–617 glasses following ISO guidelines. *Geostandards and Geoanalytical Research* 35, 397–429. https://doi.org/10.1111/j.1751-908X.2011.00120.x

Kanehira K., Banno S. & Yui S. 1975: Awaruite, heazlewoodite, and native copper in serpentinized peridotite from the Mineoka district, southern Boso peninsula. *The Journal of the Japanese Association of Mineralogists, Petrologists and Economic Geologists* 70, 388–394. https://doi.org/10.2465/ganko1941.70.388

Kantor J. 1955: Ore minerals of the Spiš-Gemer serpentinites (awaruite, heazlewoodite etc.). *Geologický Sborník Slovenskej Akadémie Vied* 3–4, 302–318 (in Slovak).

Kerrich R. & Fyfe W.S. 1981: The gold–carbonate association: source of CO_2, and CO_2 fixation reactions in Archaean lode deposits. *Chemical Geology* 33, 265–294. https://doi.org/10.1016/0009-2541(81)90104-2

Kiefer S., Majzlan J., Chovan M. & Števko M. 2017: Mineral compositions and phase relations of the complex sulfarsenides and arsenides from Dobšiná (Western Carpathians, Slovakia). *Ore Geology Reviews* 89, 894–908. https://doi.org/10.1016/j.oregeorev.2017.07.026

Kiefer S., Števko M., Vojtko R., Ozdín D., Gerdes A., Creaser R.A., Szczerba M. & Majzlan J. 2020: Geochronological constraints on the carbonate-sulfarsenide veins in Dobšiná, Slovakia: U/Pb ages of hydrothermal carbonates, Re/Os age of gersdorffite, and K/Ar ages of fuchsite. *Journal of Geosciences* 65, 229–247. http://doi.org/10.3190/jgeosci.314

Leblanc M. & Fischer W. 1990: Gold and platinum group elements in cobalt arsenide ores: Hydrothermal concentration from a serpentinite source-rock (Bou Azzer, Morocco). *Mineralogy and Petrology* 42, 197–209. https://doi.org/10.1007/BF01162691

Lexa O., Schulmann K. & Ježek J. 2003: Cretaceous collision and indentation in the West Carpathians: View based on structural analysis and numerical modeling. *Tectonics* 22, 1–16. https://doi.org/10.1029/2002TC001472

Liu Y. & Brenan J. 2015: Partitioning of platinum-group elements (PGE) and chalcogens (Se, Te, As, Sb, Bi) between monosulfide-solid solution (MSS), intermediate solid solution (ISS) and sulfide liquid at controlled fO_2–fS_2 conditions. *Geochimica et Cosmochimica Acta* 159, 139–161. https://doi.org/10.1016/j.gca.2015.03.021

Majzlan J., Mikuš T., Kiefer S. & Creaser R.A. 2022: Rhenium-osmium geochronology of gersdorffite and skutterudite–pararammelsbergite links nickel–cobalt mineralization to the opening of the incipient Meliata Ocean (Western Carpathians, Slovakia). *Mineralium Deposita* 57, 621–629. https://doi.org/10.1007/s00126-022-01101-7

Phillips G.N. & Powell R. 2010: Formation of gold deposits: a metamorphic devolatilization model. *Journal of Metamorphic Geology* 28, 689–718. https://doi.org/10.1111/j.1525-1314.2010.00887.x

Piña R., Gervilla F., Barnes S-J., Ortega L. & Lunar R. 2015: Liquid immiscibility between arsenide and sulfide melts: evidence from a LAICP-MS study in magmatic deposits at Serranía de Ronda (Spain). *Mineralium Deposita* 50, 265–279. https://doi.org/10.1007/s00126-014-0534-3

Piña R. Gervilla F., Helmy H., Fonseca R.O.C. & Ballhaus C. 2021: Partition behavior of platinum-group elements during the segregation of arsenide melts from sulfide magma. *American Mineralogist: Journal of Earth and Planetary Materials* 105, 1889–1897. https://doi.org/10.2138/am-2020-7477

Pipino G. 1980: Gold in Ligurian ophiolites, Italy. In: Panayiotou A. (Ed.): Ophiolites. *Proceedings, International ophiolite symposium, Cyprus Ministry of Agriculture and Natural Resources Geological Survey Department*, Nicosia, 765–773.

Pirajno F. 2013: Effects of metasomatism on mineral systems and their host rocks: alkali metasomatism, skarns, greisens, tourmalinites, rodingites, black-wall alteration and listvenites. In: Metasomatism and the Chemical Transformation of Rock. *Springer*, Berlin, Heidelberg, 203–251.

Pirajno F. 2015: Intracontinental anorogenic alkaline magmatism and carbonatites, associated mineral systems and the mantle plume connection. *Gondwana Research* 27, 1181–1216. https://doi.org/10.1016/j.gr.2014.09.008

Putiš M., Ivan P., Kohút M., Spišiak J., Siman P., Radvanec M., Uher P., Sergeev S., Larionov A., Méres Š., Demko R. & Ondrejka M. 2009: Meta-igneous rocks in the West-Carpathian basement, Slovakia: indicators of Early Paleozoic extension and shortening events. *Bulletin de la Société géologique de France* 180, 461–471. https://doi.org/10.2113/gssgfbull.180.6.461

Radvanec M. & Grecula P. 2016: Geotectonic and metallogenetic evolution of Gemericum (Inner Western Carpathians) from Ordovician to Jurassic. *Mineralia Slovaca* 48, 105–118.

Radvanec M. & Uher P. 2016: Platinum-group minerals in metapyroxienite from Jasov, Meliatic Unit, Slovakia. *Acta Geologica Slovaca* 8, 195–201.

Ramdohr P. 1967: A widespread mineral association connected with serpentinization. *Neues Jahrbuch für Mineralogie, Abhandlungen* 107, 241–265.

Reimann C., Ladenberger A., Birke M. & de Caritat P. 2016: Low density geochemical mapping and mineral exploration: Application of the mineral system concept. *Geochemistry: Exploration, Environment, Analysis* 16, 48–61. https://doi.org/10.1144/geochem2014-327

Rojkovič I. & Hovorka D. 1979: Relation of ore mineralization to geochemistry of the West Carpathian ultramafic massifs. *Geologica Carpathica* 30, 449–462.

Rose G., von Humboldt A. & Ehrenberg C.G. 1837: Mineralogisch–geognostische Reise nach dem Ural, dem Altai und dem Kaspischen Meere: bd. Reise nach dem mördlichen Ural und dem Altai (Vol. 1). *Verlag der Sanderschen Buchandlung (C.W. Eichhoff)*, Berlin.

Rozložník L. 1956: Report of the geological mapping of an area NE from Dobšiná. *Open-File Report, Geofond*, Bratislava (in Slovak).

Rozložník L. 1965: Analysis of the structural-metallogenic elements between Dobšiná and Mlynky. *Sborník geologických Vied, rad Západné Karpaty* 4, 29–93 (in Slovak).

Sazonov V.N. 1975: Listvenitization and ore-forming process. *Nauka*, Moscow, 1–171 (in Russian).

Schneiderhöhn H. 1944: Erzlagerstätten: Kurzvorlesungen zur Einführung und zur Wiederholung. *Gustav Fischer Verlag*, Leipzig, 1–290.

Šoštarić S.B., Palinkaš L.A., Topa D., Spangenberg J.E. & Prochaska W. 2011: Silver–base metal epithermal vein and listwaenite types of deposit Crnac, Rogozna Mts., Kosovo. Part I: Ore mineral geochemistry and sulfur isotope study. *Ore Geology Reviews* 40, 65–80. https://doi.org/10.1016/j.oregeorev.2011.05.002

Spiridonov E.M., Kulagov E.A., Serova A.A., Kulikova I.M., Korotaeva N.N., Sereda E.V., Tushentsova I.N., Belyakov S.N. & Zhukov N.N. 2015: Genetic Pd, Pt, Au, Ag, and Rh mineralogy in Noriľsk sulfide ores. *Geology of Ore Deposits* 57, 402–432. https://doi.org/10.1134/S1075701515050062

Števko M. & Sejkora J. 2020: Sb-enriched association of Ni arsenides and sulfarsenides from the Zemberg-Terézia vein system near Dobšiná (Western Carpathians, Slovak Republic). *Bulletin Mineralogie Petrologie* 28, 105–115.

Števko M., Sejkora J., Litochleb J., Macek I. & Bačík P. 2013: Krutovite and associated minerals from the Dobšiná-Teliatko occurrence (Slovak Republic). *Bulletin Mineralogie Petrologie* 21, 1–14 (in Slovak).

Tourneur E., Chauvet A., Kouzmanov K., Tuduri J., Paquez C., Sizaret S., Karfal A., Moundi Y. & El Hassani A. 2021: Co–Ni-arsenide mineralisation in the Bou Azzer district (Anti-Atlas, Morocco): Genetic model and tectonic implications. *Ore Geology Reviews* 134, 104128. https://doi.org/10.1016/j.oregeorev.2021.104128

Vozárová A., Nemec O., Šarinová K., Anczkiewicz R. & Vozár J. 2021: Carboniferous mafic metavolcanic rocks in the Northern Gemeric Unit: Petrogenesis, geochemistry, isotope composition and tectonic implication. *Geologica Carpathica* 72, 114–133. https://doi.org/10.31577/GeolCarp.72.2.3

Zoheir B. & Lehmann B. 2011: Listvenite–lode association at the Barramiya gold mine, Eastern Desert, Egypt. *Ore Geology Reviews* 39, 101–115. https://doi.org/10.1016/j.oregeorev.2010.12.002

Electronic supplementary material is available online:
Supplement S1 (EPMA analyses) at http://geologicacarpathica.com/data/files/supplements/GC-74-2-Kiefer_Suppl_S1.xlsx